IEEE Photonics Journal
An IEEE Photonics Society Publication

Open Access

Monolithic Integration of InP Wire and SiO_x Waveguides on Si Platform

Volume 7, Number 5, October 2015

H. Nishi
K. Takeda, Member, IEEE
T. Tsuchizawa
T. Fujii
S. Matsuo, Senior Member, IEEE
K. Yamada, Member, IEEE
T. Yamamoto, Member, IEEE

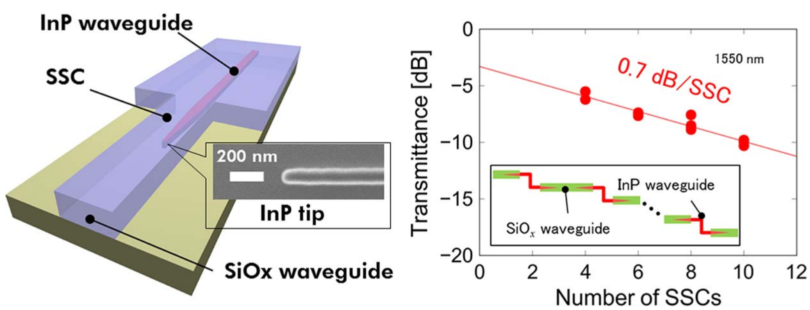

DOI: 10.1109/JPHOT.2015.2477511
1943-0655

Monolithic Integration of InP Wire and SiO_x Waveguides on Si Platform

H. Nishi,[1,2] K. Takeda,[1,2] *Member, IEEE*, T. Tsuchizawa,[1,2] T. Fujii,[1,2] S. Matsuo,[1,2] *Senior Member, IEEE*, K. Yamada,[1,2,3] *Member, IEEE*, and T. Yamamoto,[1] *Member, IEEE*

[1]NTT Device Technology Laboratories, NTT Corporation, Atsugi 243-0198, Japan
[2]Nanophotonics Center, NTT Corporation, Atsugi 243-0198, Japan
[3]National Institute of Advanced Industrial Science and Technology, Tsukuba 305-8569, Japan

DOI: 10.1109/JPHOT.2015.2477511

Manuscript received July 28, 2015; revised September 1, 2015; accepted September 1, 2015. Date of publication September 9, 2015; date of current version September 30, 2015. Corresponding author: H. Nishi (e-mail: nishi.hidetaka@lab.ntt.co.jp).

Abstract: We report a low-loss InP wire waveguide monolithically integrated with an SiO_x waveguide on an Si platform. By means of directly bonding InP to SiO_2, we realized a submicrometer-scale InP wire waveguide with high optical confinement. In addition, a several-micrometer-scale SiO_x waveguide with a refractive index difference of ~3% is integrated on the InP wire waveguide via a spot-size converter (SSC). Experimental results indicate that the InP wire waveguide has a propagation loss of 5 dB/cm and that the InP-SiO_x SSC has an insertion loss of 0.7 dB and a reflectance of less than −50 dB. By using the SSC, a low coupling loss of 0.9 dB is achieved between the optical fiber and the InP wire waveguide.

Index Terms: InP wire waveguide, Si photonics, spot-size converter, SiO_x waveguide.

1. Introduction

Over the past few decades, Si photonics technology has evolved as a promising photonic integration platform. With the goal of complete integration of passive and active photonic devices, Si and non-Si materials are being integrated on the Si photonics platform to compensate for performance disadvantage due to the physical properties of Si. In particular, for active devices, such as laser light sources and amplifiers, monolithic integration of group III–V materials on the Si platform is promising and is being intensively investigated worldwide [1]–[3]. Recently, by utilizing the high-index contrast between group III–V materials and SiO_2, III–V membrane photonic devices with a very thin III–V layer on SiO_2/Si substrate are realized [4]–[7]. For integration, the membrane devices are connected with output InP waveguides and then connected to Si photonic devices. In addition, III–V wire waveguides can be applied to nonlinear photonics thanks to high optical confinement similar to that in Si wire waveguides [8], [9].

Up to now, III–V waveguides and the integration of III–V passive and active devices have been demonstrated on an Si platform. However, there are few material options; it is either all-III–V or Si-III–V integration [1], [7]. Within their material systems, the performance of passive devices based on high-index-contrast waveguides can easily degrade because the fabrication error of core size leads to considerable variation of the effective index. In addition, for such high-index-contrast waveguides, efficient fiber coupling is an important issue. Integrations of other materials

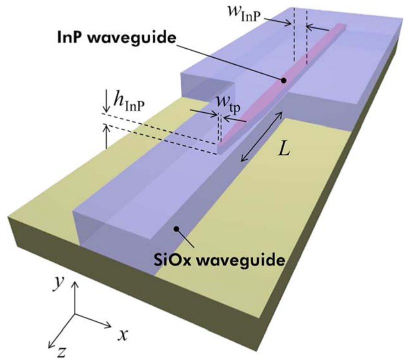

Fig. 1. Schematic of the InP-SiO_x waveguide integration structure. The SiO_2 overcladding of the SiO_x waveguide is not drawn.

can provide promising solutions to these problems. In particular, a key technology is the integration of a low-refractive-index-difference (low-Δ) [10] waveguides made of SiO_xN_y-based materials, which are suitable for high-performance passive devices [11].

In this paper, we report the monolithic integration of InP wire waveguides and low-Δ SiO_x waveguides. We form InP waveguides with sub-μm core dimensions on an SiO_2/Si substrate using the direct bonding technique. Then, using low-temperature fabrication methods, we monolithically fabricate SiO_x waveguides with 3-% Δ. To connect these two different waveguides with low loss, we use a spot-size converter (SSC) with an InP inverse-taper structure. With this integration technique, we achieve low-loss fiber coupling between a high-numerical-aperture (high-NA) single-mode fiber and the InP wire waveguide.

2. Design

Fig. 1 shows a schematic of the structure of the InP-SiO_x integration using the SSC. The InP core ($n = 3.169$) is configured on an SiO_2 undercladding ($n = 1.444$). An SiO_x layer ($n = 1.505$) covers the InP core as an overcladding. In this configuration, the InP core is completely embedded in SiO_x. The SiO_x layer is partly removed to pattern the SiO_x waveguide core. On top, a SiO_2 layer ($n = 1.468$) covers the overall structure as an overcladding of the SiO_x waveguide.

The InP waveguide has Δ of 39%, which is quite high compared with other conventional dielectric waveguides, such as silica glass, and similar to that of an Si wire waveguide (41%). Hence, the dimensions satisfying the single-mode condition are on the order of sub μm. Fig. 2 shows calculated effective refractive indices (n_{eff}) at 1550-nm wavelength for transverse-electric (TE) -like modes as a function of InP core width (w_{InP}) with various core heights (h_{InP}). The mode notations are taken from ref. [12]. For h_{InP} of 200, 300, and 400 nm, the single-mode condition can be satisfied when w_{InP}'s are less than 580, 460, and 380 nm, respectively. The dimensions satisfying the single-mode condition are slightly larger than those of Si [12].

The SiO_x core is 2×4 μm, which is one order of magnitude larger than the InP core. To connect them with low loss, in this work, we used an SSC consisting of an InP adiabatic taper and a SiO_x-waveguide core covering the taper, as shown in Fig. 1. This SSC structure is similar to the SSC for Si-SiO_x connection, which functions as a mode matching section between the InP wire and the following SiO_x waveguides [11], [13]. By tuning the taper length (L) and the tip width (w_{tp}), the propagating mode inside the InP wire could adiabatically evolve into the mode inside the SiO_x waveguide. Fig. 3(a)–(c) show calculated SSC losses as functions of w_{tp} and L with h_{InP} of 200, 300, and 400 nm, respectively. Here, the SSC loss is defined as the optical power ratio between the SiO_x waveguide output to the InP waveguide input for the fundamental TE mode at 1550-nm wavelength. For the calculation, we used a commercial software based on a two-dimensional eigenmode solver and eigenmode-expansion calculation [14]. For each h_{InP}, the SSC efficiency tends to become higher as L increases and w_{tp} decreases. When w_{tp} is too large,

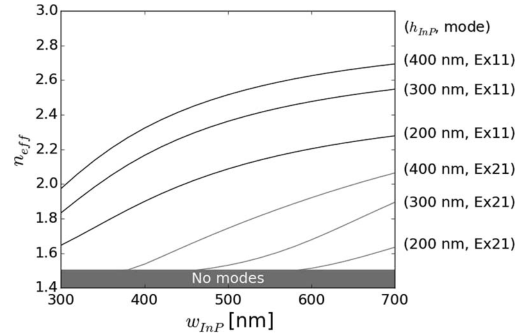

Fig. 2. Calculated effective indices (n_{eff}) of the InP waveguide modes as a function of InP core width (w_{InP}) with various InP core heights (h_{InP}).

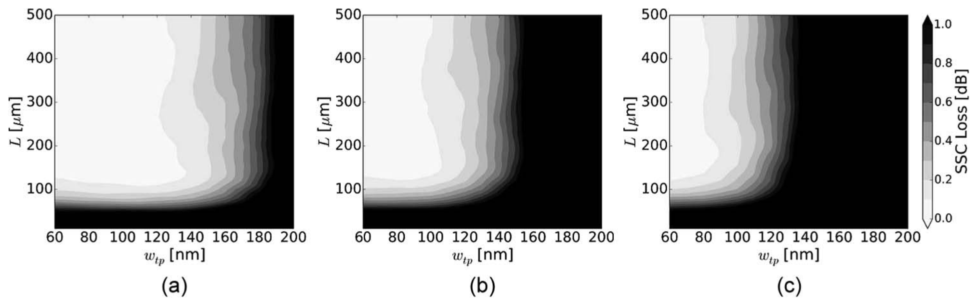

Fig. 3. Calculated SSC conversion loss as functions of taper length (L) and InP tip width (w_{tp}) with various InP core heights (h_{InP}). (a) $h_{\mathrm{InP}} = 200$ nm, (b) $h_{\mathrm{InP}} = 300$ nm, and (c) $h_{\mathrm{InP}} = 400$ nm, respectively.

the SSC efficiency can not increase even though L increases, and it reaches a low-efficiency plateau, the value of which depends on w_{tp}. This is because, with w_{tp} that is too large, the efficiency is dominated by mode mismatch at the boundary between the InP-taper tip and the SiO_x waveguide. The coupling loss between the SiO_x waveguide and the high-NA fiber was also estimated to be 0.2 dB by the calculation.

Another concern is reflection. When the SSC is integrated with a laser diode, reflected light increases oscillating-mode instability in it. Thus, the reflection at the SSC should be carefully suppressed. Fig. 4(a)–(c) show calculated reflectance at the SSC when the light was input from the InP waveguide as functions of tip width (w_{tp}) and taper length (L) with h_{InP} of 200, 300, and 400 nm, respectively. In order to achieve less than –50-dB reflectance, w_{tp} should be set to < 150, < 120, and < 100 nm for $h_{\mathrm{InP}} = 200$, 300, and 400 nm, respectively. As w_{tp} increases, the reflection at the InP tip increases. In addition, the L should be set to more than 100 μm regardless of the h_{InP} value. This is because, with L of less than 100 μm, the adiabatic mode conversion can not be achieved at the taper section, which also increases reflectance.

On the basis of these results, to confirm the single-mode propagation in the InP waveguide, we designed the InP core with dimensions of $h_{\mathrm{InP}} = 200$ nm and $w_{\mathrm{InP}} = 500$ nm. For the SSC, to confirm the low-loss connection between the InP and SiO_x waveguides, we used $w_{\mathrm{tp}} = 80$ nm and $L = 300$ μm.

3. Fabrication

In advance, we prepared two substrates: a III–V bonding substrate layered as InP/InGaAs/InP and a base substrate layered as SiO_2/Si. To prepare the III–V bonding substrate, we grew an etchstop InGaAs layer and an InP layer on InP wafer using the metal-organic vapor phase

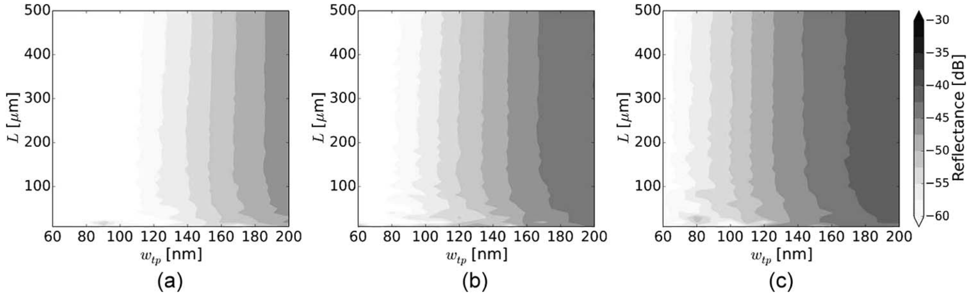

Fig. 4. Calculated SSC reflectance as functions of taper length (L) and InP tip width (w_{tp}) with various InP core heights (h_{InP}). (a) $h_{InP} = 200$ nm, (b) $h_{InP} = 300$ nm, and (c) $h_{InP} = 400$ nm, respectively.

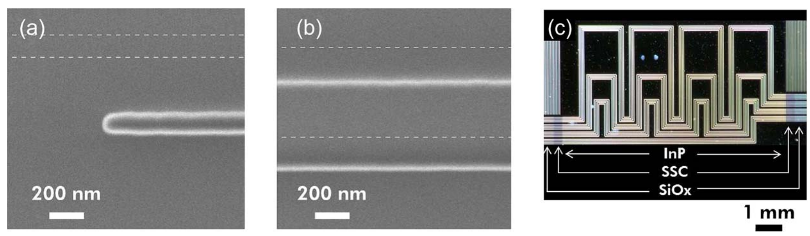

Fig. 5. SEM images of (a) InP taper tip. (b) InP core. (c) Optical microscope image of a fabricated chip.

epitaxy (MOVPE) method. The thickness of the top InP layer was set to 200 nm. The base substrate was a Si wafer with a top thermal-oxide layer of 2 μm. After surface cleaning and pre treatment, these two wafers were directly bonded by using an O_2 plasma assisted bonding technique. Then, after InP support substrate and InGaAs etch-stop layer had been removed, we obtained the InP on SiO_2 substrate. On this substrate, we deposited SiO_2 as a hard mask for InP etching and formed a resist pattern using electron-beam lithography to define the InP core and taper. Then, after the SiO_2 hard-mask pattern had been formed by reactive-ion etching (RIE), the InP core was formed by inductive-coupled-plasma (ICP) RIE. Fig. 5(a) and (b) show SEM images of a fabricated InP taper tip and InP core. The InP layer was formed with w_{tp} and w_{InP} of 137 and 551 nm, respectively. The InP width is slightly larger than designed due to the multiple etching process. Nevertheless, the single-mode condition is satisfied and SSC conversion loss is expected to be less than 0.2 dB.

Next, we fabricated SiO_x waveguides. First, a 2-μm-thick SiO_x layer was deposited by electron-cyclotron resonance (ECR) plasma-enhanced chemical vapor deposition (PECVD) [11], this was followed by definition of the low-refractive-index core of SSC to have a width of 4 μm by photolithography and RIE. In the definition of SiO_x core, the offset between InP and SiO_x cores can occur due to misalignment of our stepper lithography, which leads to polarization rotation in the SSC. Fig. 6(b) shows a calculated transmittance for the TE-like mode input to the TE-like mode output and the TE-like mode input to the TM-like mode output, as a function of misalignment defined in Fig. 6(a). Here, w_{tp} and L are set to 140 nm and 300 μm, respectively. We numerically confirmed that the polarization rotation is less than −20 dB even if the misalignment of 100 nm exists, which is a typical value on our stepper lithography. Thus, the polarization rotation is not a critical issue. Then, the SiO_2 overcladding was deposited by ECR PECVD. The processed wafer was cut by dicing to obtain facets for the fiber coupling. The facet lines cross only the SiO_x waveguide and no polishing was performed. Fig. 5(c) shows an optical microscope image of a fabricated chip. The meandering structures are InP wire waveguides with different length.

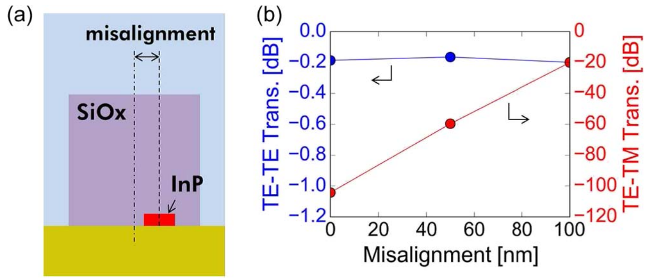

Fig. 6. (a) Definition of the misalignment. (b) Calculated transmittance for the TE-like mode input to the TE-like mode output and the TE-like mode input to the TM-like mode output as a function of misalignment.

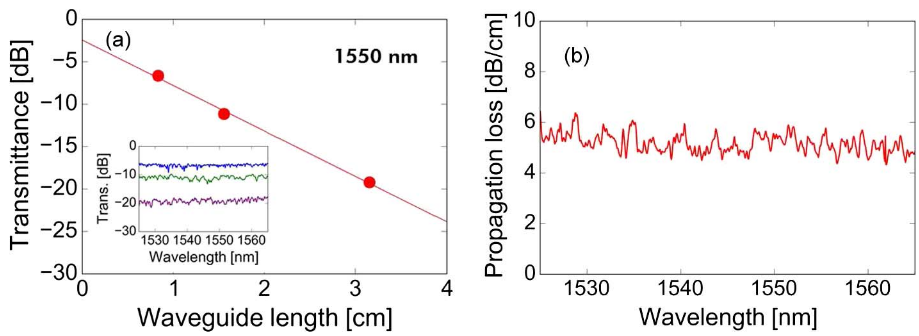

Fig. 7. Propagation characteristics of InP waveguides. (a) Waveguide transmittance as a function of InP length at a wavelength of 1550 nm. (Inset) Transmission spectra with various waveguide lengths. (b) Propagation loss spectrum estimated by the slope of fitted line in (a).

4. Experiments and Discussion

First, we characterized the propagation loss of the InP waveguide. In experiments, we used cleaved high-NA fibers that were butt-coupled with the input and output facets of the SiO_x waveguide. The input polarization was set to the TE mode. We obtained transmission spectra of the fabricated waveguides with InP-waveguide lengths of 0.83, 1.56, and 3.16 cm, respectively. Fig. 7(a) shows waveguide transmittance as a function of InP-waveguide length at 1550 nm, and the inset shows the transmission spectra of waveguides with various InP lengths. From the slope of the fitted line in Fig. 7(a), we estimated the propagation loss of 5.3 dB/cm at a wavelength of 1550 nm. In a similar way at each wavelength, we also acquired the propagation-loss spectra and obtained about 5 dB/cm within the C-band, as shown in Fig. 7(b). Note that the propagation loss of the monolithically fabricated SiO_x waveguide is 0.8 dB/cm, which is almost same performance as an unintegrated SiO_x waveguide [11].

Next, for the loss estimation of the SSC connecting the InP and SiO_x waveguides, as shown in Fig. 8(a), we measured waveguides with various numbers of InP-SiO_x connections to the SSCs. We estimated the SSC loss from the slope of the relationship between the waveguide transmittance and number of SSCs. At 1550 nm, we estimated the SSC loss to be 0.7 dB/SSC. Fig. 8(b) shows measured SSC loss as a function of wavelength. We confirmed that the SSC loss ranges from 0.6 to 1.0 dB/SSC in the C-band. The loss is slightly higher than our calculation shown in Fig. 3. This is due to scattering loss that occurred because of the surface roughness of the InP taper, which we ignored in the calculation. In addition, the fabricated taper tip was wider than the design value, which increased the SSC loss. Then, we characterized the spatial distribution of reflection in the InP-SiO_x connected waveguide using an optical low-coherence reflectometer (OLCR). For the measurement, we used a cleaved dispersion-compensated fiber (DCF) at the input facet. with index matching oil to suppress the reflection at the

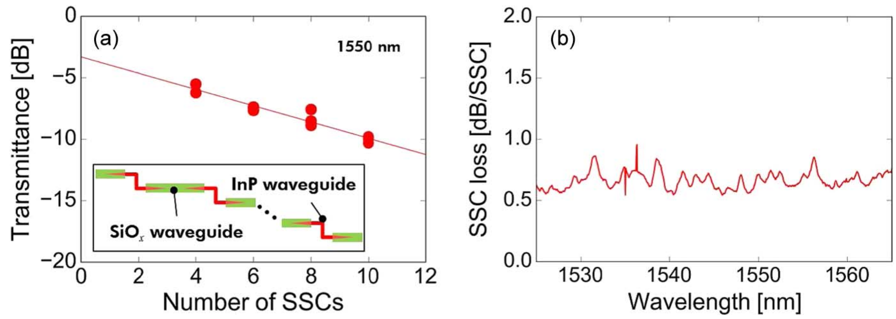

Fig. 8. Transmission characteristics of the SSC. (a) Relationship between number of SSCs and transmittance. (Inset) Test–pattern layout. (b) Estimated SSC loss spectrum.

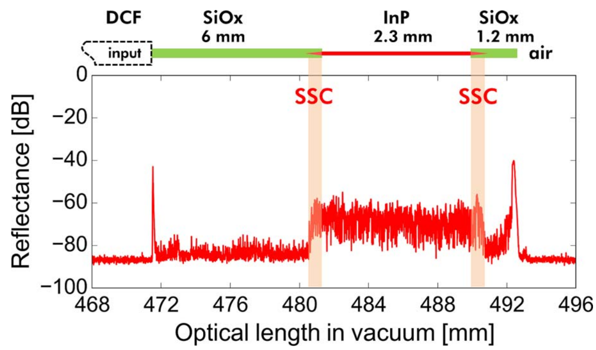

Fig. 9. OLCR trace of an InP-SiO$_x$ connected waveguide.

DCF-SiO$_x$ facet as much as possible. Fig. 9 shows a measured OLCR trace obtained with spatial resolution of 20 μm. The vertical axis was normalized by reflectance at the DCF-air boundary. No significant reflection is observed at the SSC, and the intensity of the reflection appears to be almost the same as that of back scattering from the InP waveguide. Considering DCF-SiO$_x$ coupling loss and round-trip propagation loss to the reflection point, we estimated the reflectance is less than −50 dB at the SSC. As a result, we clearly confirmed that the SSC can connect the InP waveguide and the SiO$_x$ waveguide with low loss and low reflectance. This technique can be further adopted for the monolithic integration of InP membrane active devices on Si-, Ge-, SiO$_x$-, and electronics-integrated photonic devices [15], [16].

In addition, we examined the coupling loss between the InP waveguide and a high-NA fiber. Fig. 10 shows measured coupling loss. By means of the standard method, we obtained 1.6 dB at 1550 nm by simply dividing in half the intercept on the graph of the relationship between waveguide transmittance and length as shown in Fig. 7(a). However, this 1.6 dB can be further broken down to four parts as follows: facet loss between the high-NA fiber and the SiO$_x$ waveguide, SiO$_x$ waveguide loss, SSC loss, and InP bending loss. Among them, facet loss is estimated to be 0.2 dB by the calculation. The SiO$_x$ waveguide loss was estimated to be less than 0.1 dB and negligible because the length of SiO$_x$ at the input and output is less than 1 mm and the SiO$_x$ propagation loss is 0.8 dB/cm. The SSC loss is 0.7 dB/SSC as shown in Fig. 8. These values are estimated at 1550 nm, and their variations within the C-band are negligible on the physical basis. We therefore consider that the residual 0.7 dB originates from 12 bends with a radius of 10 μm, which leads to 0.058 dB/90deg-bend. Subtracting the bending loss, we estimated the fiber-to-InP-waveguide coupling loss to be only 0.9 dB at wavelength of 1550 nm as shown in Fig. 10.

Finally, we compare the obtained characteristics with existing reports using Table I. Concerning to the propagation loss, our waveguide exhibits preferably low loss among sub-μm-wide

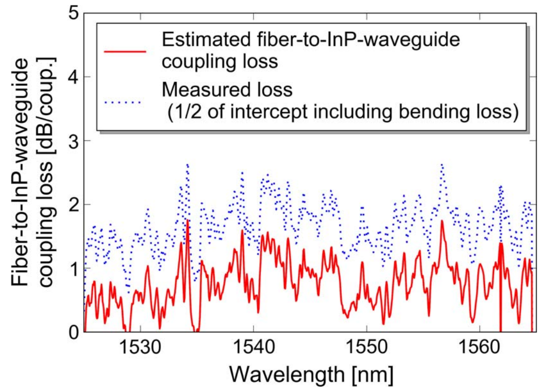

Fig. 10. Measured coupling loss from a high-NA fiber to the InP waveguide as a function of wavelength.

TABLE I
Comparison of III–V Wire Waveguides on Si Platform

Bonding method	Core	Core dimensions $w \times h$ [nm]	Prop. loss [dB/cm]	Fiber coup. loss [dB/coup.]	Ref.
Direct (InP/SiO_2)	InP	560×200	5.2	0.9 (high-NA fiber)	This work
Direct (SiO_2/SiO_2)	GaAs	400×400	45	13.5 (lense fiber)	[17]
Direct ($InGaAsP/SiO_2$)	InGaAsP	2000×315	30	4.2	[19] [20]
Direct (Al_2O_3/Al_2O_3)	InP/InGaAsP	2000×375	4	-	[7]
Adhesive (BCB/SiO_2)	InP	400×250	3.3	6.4	[6] [18]
Adhesive (BCB/SiO_2)	GaInAsP	410×150	4	-	[21]
Adhesive (BCB/SiO_2)	InGaP	630×250	12	7.5	[8]

waveguides fabricated by the direct bonding technique. Among the waveguides fabricated by the direct bonding technology, a lower propagation loss is reported [7]. However, this structure has a much larger core width of 2000 nm, whereas we use a sub-μm core width, which makes a direct comparison of the loss values difficult. We believe the propagation loss of our waveguide can be further decreases by improving the bonding process, bonding structure, and the techniques for III–V nanofabrication on the Si platform. For adhesively bonded waveguides, lower loss than this work, comparable to that of Si wire waveguides in early days has been reported [6], [18], [21]. However, the fact that our concept relies on direct bonding instead of adhesive bonding makes it highly promising for cost-effective mass fabrication of III–V devices monolithically integrated on $\geq$ 300-mm Si wafers and subsequent processing using standard microelectronic CMOS manufacturing facilities [4]. For that purpose, the high-temperature processes needed for III–V crystal growth and activation annealing are performed in the front-end-of-line (FEOL). If adhesive bonding technology is used for III–V integration it would be difficult to carry out such high-temperature processes. Therefore, we consider the direct bonding technology is promising.

As for the fiber coupling loss, to the best of our knowledge, the lowest coupling loss from a standard single-mode fiber (SMF) to the InP waveguide on the Si platform is 4.2 dB/coupling with a grating coupler [20]. Even though we used a high-NA fiber in this work, we expect the SMF-to-InP-waveguide coupling of around 1 dB can be achieved thanks to the low-loss InP-SiO_x SSC. Because a high-NA fiber can be connected with SMF with only 0.2-dB loss by the thermally-expanded-core process and the fiber-fusion splicing. We have previously reported an SSC for the SMF to Si-wire waveguide coupling [23]. Moreover, the SSC provides a wide operation bandwidth of over 40 nm as shown in Fig. 8 and this bandwidth potentially exceeds over 100 nm [22].

We believe this low-loss and broadband fiber coupling technique is very useful for the membrane lasers on Si and their wavelength-division-multiplexing application and for the nonlinear application of the III–V wire waveguides.

5. Conclusion

By means of the direct bonding technique, an InP wire waveguide with propagation loss of 5 dB/cm in the C-band was developed on an Si platform. In addition, we monolithically integrated the InP wire waveguide and an SiO_x waveguide and achieved a 0.7-dB connection between InP wire and SiO_x waveguides via a SSC with low reflectance of less than −50 dB. Moreover, using the SSC, we achieved low-loss fiber coupling. This work is a first step for the integration of III–V active devices with the Si-, Ge-, SiO_xN_y-, and electronics-integrated photonic circuits.

Acknowledgment

The authors thank Dr. R. Kou, Mr. T. Hiraki, Dr. K. Takeda, and Dr. K. Okazaki for helpful discussions and Dr. S. Kodama for his support.

References

[1] G. Roelkens *et al.*, “III-V/silicon photonics for on-chip and intra-chip optical interconnects,” *Laser Photonics Rev.*, vol. 4, no. 6, pp. 751–779, Nov. 2010.
[2] A. Descos *et al.*, “Heterogeneously integrated III-V/Si distributed Bragg reflector laser with adiabatic coupling,” in *Proc. ECOC*, 2013, pp. 1–3, Th.1.B.2.
[3] C. Zhang *et al.*, “Low threshold and high speed short cavity distributed feedback hybrid silicon lasers,” *Opt. Exp.*, vol. 22, no. 9, pp. 10202–10209.
[4] S. Matsuo *et al.*, “Directly modulated buried heterostructure DFB laser on SiO_2/Si substrate fabricated by regrowth of InP using bonded active layer,” *Opt. Exp.*, vol. 22, no. 10, pp. 12139–12147, 2014.
[5] S. Matsuo *et al.*, “Directly modulated DFB laser on SiO_2/Si substrate for datacenter networks”, *J. Lightwave Technol.*, vol. 33, no. 6, pp. 1217–1222, Mar. 2015.
[6] J. van der Tol *et al.*, “Photonic integration in Indium-Phosphide Membranes on Silicon (IMOS),” in *Proc. SPIE*, vol. 8988, Mar. 2014, Art ID. 89880M.
[7] Y. Ikku *et al.*, “Low-driving-current InGaAsP photonic-wire optical switches using III-V CMOS photonics platform,” *Opt. Exp.*, vol. 20, no. 26, pp. B357–B364, Dec. 2012.
[8] U. Dave *et al.*, “Nonlinear properties of dispersion engineered InGaP photonic wire waveguides in the telecommunication wavelength range,” *Opt. Exp.*, vol. 23, no. 4, pp. 4650–4657, Feb. 2015.
[9] M. Pu *et al.*, “AlGaAs-on-insulator nanowire with 750 nm FWM bandwidth, −9 dB CW conversion efficiency, and ultrafast operation enabling record Tbaud wavelength conversion,” in *Proc. OFC*, 2015, vol. 1, pp. 1–3, Th5A.3.
[10] K. Okamoto, *Fundamentals of Optical Waveguides*, 2nd ed. London, U.K.: Academic, 2006.
[11] T. Tsuchizawa *et al.*, “Monolithic integration of silicon-, germanium-, and silica-based optical devices for telecommunications applications,” *IEEE J. Sel. Top. Quantum Electron.*, vol. 17, no. 3, pp. 516–525, May 2011.
[12] K. Yamada, “Silicon photonic wire waveguides: Fundamentals and applications,” in *Silicon Photonics II*, D. Lockwood and L. Pavesi, Eds. Berlin, Germany: Springer-Verlag, Ch. 1.
[13] T. Shoji, T. Tsuchizawa, T. Watanabe, K. Yamada, and H. Morita, “Low loss mode size converter from 0.3 um square Si wire waveguides to singlemode fibres,” *Electron. Lett.*, vol. 38, no. 25, pp. 1669–1670, Dec. 2002.
[14] *FIMMWAVE/FIMMPROP*, Photon Design Inc., Oxford, U.K.
[15] H. Nishi *et al.*, “Monolithic integration of a silica-based arrayed waveguide grating filter and silicon variable optical attenuators based on p-i-n carrier-injection structures,” *Appl. Phys. Exp.*, vol. 3, no. 10, Oct. 2010, Art ID. 102203.
[16] H. Nishi *et al.*, “Monolithic integration of a silica AWG and Ge photodiodes on Si photonic platform for one-chip WDM receiver,” *Opt. Exp.*, vol. 20, no. 8, pp. 9312–9321, Apr. 2012.
[17] R. Kafouf *et al.*, “Ultrahigh relative refractive index contrast GaAs nanowire waveguides,” *Appl. Phys. Exp.*, vol. 1, no. 12, 2008, Art ID. 122101.
[18] Y. Jiao *et al.*, “Fullerene-assisted electron-beam lithography for pattern improvement and loss reduction in InP membrane waveguide devices,” *Opt. Lett.*, vol. 39, no. 6, pp. 1645–1648, Mar. 2014.
[19] M. Takenaka, M. Yokoyama, M. Sugiyama, Y. Nakano, and S. Takagi, “InGaAsP photonic wire based ultrasmall arrayed waveguide grating multiplexer on Si wafer,” *Appl. Phys. Exp.*, vol. 2, no. 12, 2009, Art ID. 122201.
[20] M. Takenaka, M. Yokoyama, M. Sugiyama, Y. Nakano, and S. Takagi, “InGaAsP grating couplers fabricated using complementary-metal-oxide-semiconductor-compatible III-V-on-insulator on Si,” *Appl. Phys. Exp.*, vol. 6, no. 4, 2013, Art ID. 042501.
[21] J. Lee *et al.*, “Low-loss GaInAsP wire waveguide on Si substrate with benzocyclobutene adhesive wafer bonding for membrane photonic circuits,” *Jpn. J. Appl. Phys.*, vol. 51, no. 4R, Mar. 2012, Art ID. 042201.
[22] T. Tsuchizawa *et al.*, “Microphotonics devices based on silicon microfabrication technology,” *IEEE J. Sel. Top. Quantum Electron.*, vol. 11, no. 1, pp. 232–240, Jan. 2005.
[23] H. Nishi, T. Tsuchizawa, H. Fukuda, H. Okayama, and K. Yamada, “Connection of Si-wire waveguides with singlemode fibers by inverse-taper spot-size converters,” in *Proc. ISPEC*, 2014, P-50.